Article

Preferential Binding of Cytochrome c to an Anionic Ligand-Coated Gold Nanoparticle: A Complementary Computational and Experimental Approach

Emily J Tollefson, Caley R Allen, Gene Chong, Xi Zhang, Nikita D. Rozanov, Anthony Bautista, Jennifer J. Cerda, Joel A. Pedersen, Catherine J. Murphy, Erin E. Carlson, and Rigoberto Hernandez

ACS Nano, **Just Accepted Manuscript** • Publication Date (Web): 13 May 2019

Preferential Binding of Cytochrome *c* to Anionic Ligand-Coated Gold Nanoparticles: A Complementary Computational and Experimental Approach

Emily J. Tollefson[1] †, Caley R. Allen[2] †, Gene Chong[2], Xi Zhang[3], Nikita D. Rozanov[2], Anthony Bautista[2], Jennifer J. Cerda[1], Joel A. Pedersen[4,5], Catherine J. Murphy[3], Erin E. Carlson[1], and Rigoberto Hernandez[2*]*

[1]Department of Chemistry, University of Minnesota – Twin Cities, Minneapolis, MN 55455, United States

[2]Department of Chemistry, Johns Hopkins University, Baltimore, MD 21218, United States

[3]Department of Chemistry, University of Illinois at Urbana – Champaign, Urbana, IL 61801, United States

[4]Environmental Chemistry and Technology Program, University of Wisconsin – Madison, Madison, WI 53706, United States

[5]Department of Chemistry, University of Wisconsin – Madison, Madison, WI 53706, United States

† These authors contributed equally to the work.

*** Corresponding Authors:**
Rigoberto Hernandez; r.hernandez@jhu.edu
Erin Carlson; carlsone@umn.edu

ABSTRACT

Membrane-bound proteins can play a role in the binding of anionic gold nanoparticles (AuNP) to model bilayers; however, the mechanism for this binding remains unresolved. In this work, we determine the relative orientation of the peripheral membrane protein cytochrome *c* in binding to a mercaptopropionic acid-functionalized AuNP (MPA-AuNP). As this is non-rigid binding, traditional methods involving crystallographic or rigid molecular docking techniques are ineffective at resolving the question. Instead, we have implemented a computational assay technique using a cross-correlation of a small ensemble of 200 ns long molecular dynamics trajectories to identify a preferred non-rigid binding orientation or pose of cytochrome *c* on MPA-

AuNPs. We have also employed a mass spectrometry-based footprinting method that enables the characterization of the stable protein corona that forms at long time-scales in solution but remains in a dynamic state. Through the combination of these computational and experimental primary results, we have established a consensus result establishing the identity of the exposed regions of cytochrome *c* in proximity to MPA-AuNPs and its complementary pose(s) with amino-acid specificity. Moreover, the tandem use of the two methods can be applied broadly to determine the accessibility of membrane binding sites for peripheral membrane proteins upon adsorption to AuNPs, or to determine the exposed amino-acid residues of the hard corona that drive the acquisition of dynamic soft coronas. We anticipate that the combined use of simulation and experimental methods to characterize biomolecule-nanoparticle interactions, as demonstrated here, will become increasingly necessary as the complexity of such target systems grows.

KEYWORDS: gold nanoparticle, molecular dynamics simulations, cytochrome *c*, lysine modification, protein footprinting, mass spectrometry

Nanomaterials have a large and growing socioeconomic impact on industrial and academic fields for their emerging use in applications from energy to medicine. They are often designed for a specific function; however, understanding of the short- to long-term environmental effects of these synthetically engineered nanoscale objects on biological systems and their molecular-scale components, such as phospholipid bilayers and proteins is limited. As an example, when nanoparticles (NPs) interact with proteins, they might alter the protein's secondary, tertiary, or quaternary structures critical to protein functionality, causing unexpected organismal stress, toxicity or other unanticipated biological consequences.[1]

It is well established that the characteristics of NPs, such as their composition, size, and ligand coating, are crucial to their interactions with proteins and other biomolecules.[2] Both computational modeling and advances in the experimental synthesis of NPs have enabled controlled synthesis of NP shape, size, and surface chemistry to probe NP surface-specific interactions with biomolecules and predict NP toxicity[3,4] yet experimental characterization of the nano-bio interface with high molecular-level sensitivity has been limited. A wide variety of direct and indirect methods exist to examine protein-NP interactions.[5,6] Experiments have focused largely on the acquisition of a protein corona by NPs, more generally, and its effect on cytotoxicity.[7-11] To confidently identify specific amino acid residues involved in protein-NP interactions, NMR and mass spectrometry have been employed.[5,12,13] While information-rich, NMR-based methods often require extensive expertise, high concentrations, and can only be used on relatively small proteins at sufficiently high concentrations. Instead, we turned our attention to mass spectrometry-based methods that have been developed to determine the specific residues responsible for interaction between biomolecules, called protein footprinting.[14,15] Protein footprinting utilizes the differential solvent accessibility of amino acids in a free protein relative to a protein that is complexed with another biomolecule or material. This technique has been widely utilized to study many processes such as protein-protein and protein-ligand interactions and has been successfully applied to protein-NP systems.[16-19] For example, Dordick and co-workers[17] utilized lysine-specific acylation coupled with matrix assisted laser desorption-ionization time of flight tandem mass spectrometry (MALDI-TOF MS/MS) to propose which faces of cytochrome *c*, RNase A, and lysozyme interacted with 4 and 15 nm silica nanoparticles. When paired with molecular dynamics (MD) simulations, protein footprinting can be used as a robust experimental technique to determine the accuracy of the predicted models of protein-nanoparticle interactions and assist in improving simulations;

likewise, the computational models can provide deeper insight into conformational information that cannot be probed by surface accessibility experiments alone.

Molecular dynamics (MD) simulations at all-atom to coarse-grained scales has emerged as a useful tool for exploring non-static binding partners such as that involving a protein (or proteins as in corona formation) and a nanoparticle.[20-24] The difficulty in identifying the preferred orientation of biomolecules towards a given NP using MD simulations is exacerbated by the near degeneracy of many putative binding sights on the NP due to the self-similarity —if not quite uniformity— of the NP. Nevertheless, if one samples the initial conditions sufficiently to remove biases that could lead to local minima in the binding process, one can predict properties of the protein-NP system such as protein face- and amino acid-specific interactions with NP ligands that drive the formation and structuring of coronas on NPs. The corresponding experiments to such simulations have thus far confirmed the general orientation of proteins on NPs *via* NMR[25,26] and the presence of salt-bridge formation between carboxylate-terminated NP ligands and ammonium groups, as present in the amino acid lysine, *via* infrared spectroscopy.[27] In the present work, the amino acid residue-specific interactions predicted by simulation for a protein-NP system were validated experimentally using mass spectrometry-based protein footprinting. We establish protein footprinting as a complementary experimental technique to identify preferential binding of proteins to NPs and reduce the number of initial starting configurations needed for simulations.

Specifically, we examine the model system of horse heart cytochrome *c* (cyt *c*) and 4 nm 3-mercaptopropionic acid (MPA) coated gold NPs (AuNPs)—which we call MPA-AuNP throughout this work. Cyt *c* associates with anionic lipid domains in the inner mitochondrial membrane and

is directly involved in the electron transport chain when bound to the membrane and indirectly in cell apoptosis when removed from the membrane.[28] The exact location of the anionic phospholipid hosting region(s) in cyt *c* and, therefore, the final orientation(s) of the protein on bilayers containing anionic phospholipids has been highly debated,[29,30] and some of us recently suggested a possible resolution.[31] Specifically, the degree of binding between cyt *c* and the lipid bilayer was found to exhibit preferred orientational binding sites in cyt *c*, and to vary depending on the model bilayer composition.[31] Experiments have shown that MPA-AuNPs only weakly associate with supported lipid bilayers[32] but associate strongly in the presence of cyt *c* on bilayers proportional to the number of cyt *c* bound to the bilayer.[31] AuNPs coated with polyacrylic acid were also found to remove a small population of cyt *c* weakly bound to the bilayer.[31] These results suggest a preferred cyt *c* orientation such that cyt *c* stably associates with the membrane, exposing a face to solvent that preferentially attracts MPA-AuNPs, and a potentially interfering role of anionic NPs in the regulatory membrane (dis)association of cyt *c*.

Here, we are interested in pursuing this question through a complementary approach by investigating the degree to which a membrane binding protein, cyt *c*, binds regiospecifically to the nanoparticle, rather than the bilayer. To this end, we will make reference to the binding sites[33-35] of cyt *c* to anionic cardiolipin-containing lipid domains: site N (Phe36, Gly37, Thr58, Trp59, Lys60), site A (Lys72, Lys73, Lys86, Lys87), site C (Asn52), and site L (Lys22, Lys25, His26, Lys27, His33). If there is to be binding between the three components —nanoparticle, cyt *c*, and the bilayer— then the exposure of cyt *c* to an NP would in turn also need to be preferentially oriented. Thus, the aim of this work is to interrogate the binding of cyt *c* to NP so as to establish

the nature of their mutual binding interaction and its implications on three-body interactions, such as in the case of cyt *c*-assisted binding between NPs and a bilayer.

The MD simulations reveal the preferred non-rigid binding orientation of the peripheral membrane protein cyt *c* on anionic AuNPs that persists in the AuNP hard corona at long time-scales, as confirmed by mass spectrometry-based footprinting experiments. The combined bottom-up modeling and protein footprinting methodology also reveals the consequent corresponding solvent-accessible protein faces and amino acids. The latter are available to drive the acquisition of additional biomolecules in the formation of a soft corona,[9,36-38] and to preferentially bind to anionic membranes.[31] We thereby infer the possible preferred organizational structure of NP-cyt *c*-membrane complexes with biological implications due to potential NP interference in cyt *c* (dis)association from membranes which forms a prediction of this work. Our integrated approach can be applied to NPs and proteins, each with a broader range of surface chemistries, to develop a database and an associated set of design rules for the interaction between NPs and proteins, and represents an important strategy for the mapping of related systems.

RESULTS AND DISCUSSION

Cytochrome *c* Structure and Orientation with Mercaptopropionic Acid (MPA)-Functionalized AuNPs (MPA-AuNPs). Despite being perhaps the most thoroughly investigated peripheral membrane protein, the full characterization of the preferred binding of cyt *c* to arbitrary nanoscale constructs such as membranes or nanoparticles is incomplete. Absent crystal structures of cyt *c* bound to MPA-AuNP (which may not be possible because the binding may not be rigid), the precise site(s) or preferred binding orientation(s) on MPA-AuNPs can nevertheless be assessed *via* atomistic molecular dynamics (MD) simulations. Sites A, C, L, N (**Figure 1**), and several

lysine residues have been implicated as possible candidates for the non-rigid binding site of cyt *c* to MPA-AuNP. [29,30,39-43] n our MD simulations, we focused on observables that characterize their relative positions. For simplicity, we labeled six opposing faces of cyt *c* by associating each with a plane of a cube, and arbitrarily chose Face 1 to be one that was particularly electropositive. Specifically, the residues that are closest to this plane are Gly37, Arg38, Lys60, Glu61, Glu62, Lys99. The orientation around Face 1 was constrained by choosing Face 2 to be identified with Glu66, Glu69, Asn70, Lys73, Lys87, and Arg91. The remaining planes were then associated as follows: Face 3 with Thr48, Thr49, Asp50, Ala51, Lys53, and Asn54; Face 4 with Asp2, Val3, Glu4, Lys5, Lys7, and Lys8; Face 5 with Glu21, Lys22, Gly23, Gly24, Lys25 and His26; and Face 6 with Lys13, Gln16, Thr28, Lys72, Lys79, and Ile81. We ran six molecular dynamics trajectories, each with a different face of cyt *c* facing the MPA-AuNP as the starting orientation (**Figure 2**).

Figure 1. Representative initial orientation of cytochrome *c* (cyt *c*) near the 4 nm mercaptopropionic acid-functionalized AuNP (MPA-AuNP). The five centers of mass (COMs) on cyt *c* (shown to the right of the MPA-AuNP) used to monitor the distances Δx to the bare AuNP surface are color coded for site A (green), site C (orange), site L (blue), site N (red), and the cyt *c* (black) COM. In the MPA-AuNP, gold atoms are shown as orange beads, and the ligands are shown as a stick model highlighting sulfur atoms, oxygen atoms, and the carbon chains in yellow, red, and cyan, respectively. Note: the MPA ligand layer is ~5 Å, and this distance can be subtracted from Δx to obtain distance from the ligand-coated AuNP surface.

Figure 2. The starting orientations of cyt *c* around the MPA-AuNP for Trajectories 1-6, as labeled by the face of the protein and corresponding die shown coming out of the page to the reader. The face of the protein initially pointing towards the NP is indicated by the face of the bottom of the die. For example, trajectory 1 has face 2 initially pointing towards the NP, and that face can be seen from the initial structure of trajectory 2. The color scheme representing the COMs of the cyt *c* binding sites and the atoms and ligands on MPA-AuNP is the same as in **Fig. 1**. Sodium ions are shown as gray beads.

Relative Orientation of Cytochrome *c* in Close Proximity to MPA-AuNPs. The relative orientation of cyt *c* in each of the trajectories was tracked using the relative distance between the COMs of selected sites and the bare AuNP surface shown in **Figure 1**. The values of these figures of merit along the trajectories from a representative sample of initial orientations of cyt *c* are shown in **Figure 3** and correspond to the structures shown in **Figure 2** and in **Figure S1.2** in the Supporting Information. The steady descent of the cyt *c* COM towards the AuNP surface suggests non-rigid association of the protein with the AuNP. The three trajectories not shown here either had the cyt *c* effectively remain in the initial orientation (either near site A or site L), or did not quite relax to any structure within the 200 nanosecond simulation. The three shown here display relaxation from different orientations, and all three settle into configurations with either site A or L facing the MPA-AuNP, suggesting that they are the preferred non-rigid binding orientations. In some trajectories, cyt *c* reaches a minimum in which site L drives the binding but site A is not quite on the opposite end. Further detail on the orientation is captured in **Figures 4** and **5**, which show the distances from specific residues on sites A and L, respectively. Lysine residues that are within 10 Å of the AuNP surface suggest salt-bridge formation with the MPA ligand layer. In those trajectories which lead to structures with good overall binding for site A, residue K86 is closest to MPA-AuNP. This does not necessarily mean that the interaction between K86 and the NP is driving the binding because it is the totality of the interactions facing the NP for the preferred orientations of cyt *c* that drives the binding. However, the tendency for the proximity of K86 does suggest specificity in the relative orientation of the binding. That is, the contact is nearly centered at residue K86 for site A, whereas all of the residues associated with site L are in near proximity, including K22. Both of these sites are accessible through the footprinting methods being used experimentally in this work (*vide infra*).

Figure 3. The distance Δx between the COM positions of the cyt *c* binding sites and the MPA-AuNP surface, as highlighted in **Fig. 1**, are monitored for trajectories 3, 4, and 6. The green, blue, orange, red, and black curves are the measured distances between the bare AuNP surface and the COM of site A, site L, site C, and site N or the cyt *c* COM, respectively.

Figure 4. The distance Δx between the specific groups of amino acids—residues K72, K73, K86, and K87, and the COM of site A—in the anionic phospholipid binding site A of cyt *c* and the surface of the MPA-AuNP for trajectories 3, 4, and 6.

Figure 5. The distance Δx between the specific groups of amino acids—residues K22, K25, K26, K27 and K33, and the COM of site L—in the anionic phospholipid binding site L of cyt *c* and the surface of the MPA-AuNP for trajectories 3, 4, and 6.

Cytochrome *c* Secondary and Tertiary Structure Conformations. While the relative distance and orientation of cyt *c* to the MPA-AuNP surface were revealed through the simulations reported in the previous section, these do not clearly tell us which of the two local minima—with binding at sites A or L— is preferred. To help resolve this question, we monitored the radius of gyration as shown in **Figure 6** and RMSD of cyt *c* as shown in **Figure S1.8** throughout the 200 ns trajectories. As a control on the size of the protein, we ran a 200 ns trajectory of cyt *c* solvated by the same density of TIP3P waters as used in the protein-NP simulations, and provide those values in **Figure S1.3** in the SI. As seen there, the radius of gyration, R_g, of the free cyt *c* in solution is approximately 13.6 Å in agreement with the experimentally observed value[44] at 13.5 Å. The trajectories that bind to site L, such as that from trajectory 3 (**Figure 3,5a**), remain at R_g values comparable to that of the free protein. On the other hand, in the case of the structures binding at site A (from trajectories 4 and 6, **Figure 4b,c**), both the R_g and RMSD increase as cyt *c* approaches the MPA-AuNP, suggesting the proteins open up in response to an interaction with the MPA-

AuNP. This further suggests that non-rigid binding at site A may be strengthened by internal energy changes (which compensate for the internal restructuring), while the non-rigid binding at site L is driven by entropic considerations (which permit a large set of orientations to be stable.) This finding in the simulations agrees with the experimental observations in that both sites are found to have some degree of non-rigid binding, and the specific sites exposed to solvent in the final configurations seen here correspond to those seen to be available in the footprinting results (*vide infra*). In all trajectories, the RMSD values for the heme group remain nearly constant throughout the trajectory, and the heme group is not directly involved in binding, as previously shown in simulations of cyt *c* on Ag surfaces.[43]

Figure 6. The radius of gyration R_g of cyt *c vs*. time along each 200 ns MD trajectory (right panels) as a function of the distance Δx between the cyt *c* COM and the surface of the MPA-AuNP (left panels).

Cytochrome *c* Circular Dichroism. The secondary and tertiary structure of both free cyt *c* in water and cyt *c* adsorbed on MPA-AuNPs were examined by circular dichroism (CD).[45] The far-UV CD spectra of free cyt *c* has two negative peaks at 208 and 222 nm, corresponding to the helical character of the protein **(Figure 7**).[46] The ratio of the 222 nm and 208 nm signal can be utilized to evaluate the α-helices of proteins.[47] Canonical α-helixes have an expected range of 1.25–1.75.[48] The 222/208 nm ratio is 1.72 in free cyt *c* and corresponds to reported CD spectra of cyt *c*.[49-53] In comparison, while cyt *c* incubated with MPA-AuNPs exhibits minima at the same wavelengths, the global minimum has switched from 222 nm to 208 nm, resulting in a lowered 222/208 nm ratio of 0.77. A similar shift, while not as pronounced, has been observed in studies of cyt *c* adsorbed to multiwall carbon nanotubes and glutathione-capped AuNPs.[49,53]

Figure 7. Circular dichroism spectra for cyt *c* free and incubated with MPA-AuNPs. The CD spectra of free cyt *c,* 4 μM in H_2O (pH 8.6), is shown in black and cyt *c* + MPA AuNP (18 nM) is shown in red.

To estimate the percent composition of secondary structures, the CD spectra were further deconvoluted using CONTIN (**Figure 8**).[54] The regular α-helix composition decreased upon adsorption to MPA-AuNPs (28% *versus* 17%). A corresponding increase was calculated in the content of distorted α-helix structures (8% *versus* 12%) and regular β-sheet content (3% *versus* 12%). Increase in β-sheet composition of cyt *c* has been reported to correlate to conformational changes, which increase exposure of the heme site.[55] Taken in combination with the protein deformation observed in the molecular dynamics simulations (*vide supra*), the secondary and tertiary structure of cyt *c* are distorted upon interaction with MPA-AuNPs.

Figure 8. Secondary structure calculations. Contributions to cyt *c* secondary structure were determined by fitting CD spectra using CONTIN. Contributions from regular α-helix, distorted α-helix, regular β-sheet, distorted β-sheet, turn, and unordered are shown in black for free cyt *c* and red for cyt *c* incubated with MPA-AuNP.

Cytochrome *c* Lysine-Specific Protein Footprinting. The binding sites indicated to be important for particle interaction by the molecular dynamics simulations are all lysine-based. Previous studies of cyt *c*-nanoparticle systems have identified that the electrostatic interaction of lysine residues with negatively charged ligands is important.[17-18,43,49-52] In addition, lysine residues have been found to have a higher propensity to penetrate the NP surface-bound water layer due to their flexible side chain, thereby facilitating binding.[43] Dordick and co-workers[17] determined site A preferentially interacted with 4 and 15 nm silica NP. However, in a previous report Dordick and

co-workers[50] did not observe a change in cyt *c* structure upon adsorption to 4 nm silica NPs, but did for larger NPs. The preferential binding of both sites A and L in cyt *c* observed in our simulations and the deformations observed by both simulation and CD experiments suggest that the binding interactions are likely not the same with 4 nm MPA-AuNPs.

To interrogate preferential binding, we utilized lysine-specific protein footprinting.[14] This strategy enables the identification of lysine residues that are differentially accessible in the native *versus* nanoparticle-bound forms of cyt *c*. This is accomplished by acetylation of only solvent accessible residues followed by characterization of the extent to which each lysine is modified using mass spectrometry-based methods (**Figure S2.9**). Lysine acetylation with acetic anhydride is not suitable for a buffer-free system, as acetic acid is produced and would decrease the pH. Instead, we labeled with *N*-acetoxy-succinimide, which has a neutral by-product.[56] At neutral pH, labeling was not observed, even at 10,000 molar equivalents of *N*-acetoxy-succinimide (data not shown). The pI of cyt *c* is 10.4;[57] to increase labeling, the pH was adjusted to 8.6, at which the MPA carboxylic acids will be negatively charged while the majority of lysine residues will remain positively charged. To determine if the basic pH would alter the structure of cyt *c*, CD spectra at both neutral pH and pH 8.6 were collected and found to be the same (**Figure S2.6**), consistent with previous studies which found no structural change in cyt *c* between pH 3 and 12.[58]

TEM measurements reveal the MPA-AuNPs have a core diameter of 4.5 ± 1.2 nm (**Figure S2.2**); however, DLS measurements of 19.6 ± 0.3 nm indicate a degree of nanoparticle aggregation. To minimize protein-protein interactions that would confound our ability to directly determine protein-NP interactions, we sought to determine an appropriate concentration of cyt *c* to AuNP.

We determined the number of cyt *c* adsorbed per MPA-AuNP aggregate to be 9 and 15 at 50% saturation by dynamic light scattering and UV-Vis, respectively (**Figure S2.5**).[59] A colorimetric titration with indicated monolayer coverage was reached between 20 to 40 cyt *c* to MPA-AuNP aggregate (**Figure S2.6**); therefore, we utilized a ratio of 10:1 cyt *c* to MPA-AuNP. Finally, to ensure recovery of the entire protein from the nanoparticle, we dissolved the AuNP with a solution of potassium cyanide (KCN) before digestion of the protein with chymotrypsin.[60]

Chymotrypic digests of labeled cyt *c* and of labeled cyt *c* from complexes with MPA-AuNPs were subjected to nanoLC-MS/MS for peptide mapping. These data were analyzed by PEAKS 8.5 PTM profiling (Bioinformatics Software Inc).[61] There was a decrease in modification upon incubation with MPA-AuNPs for all three lysine residues in site L (**Figure 9**: K22, K25, K27), in addition to K86 of site A and K79, indicating decreased solvent accessibility either due to particle binding or protein deformation. On the other hand, two lysine residues in site A (K72 and K73), as well as K39 exhibited an increase in acetylation, and therefore solvent accessibility, suggesting they are not integral in the interaction of cyt *c* with 4 nm MPA-coated AuNP. This also implies that these residues may become more solvent exposed due to protein deformation on the NP surface. Examination of the location of the lysine residues—illustrated in **Figure 10**—with decreased acetylation upon interaction with MPA-AuNP reveals that they are close in space. Nakano and co-workers[62] have previously identified K13, K25, K27, K79, and K86—of which K25 and K27 are associated with site L and K86 is associated with site A—as the probable interaction site of cyt *c* with 11-mercaptoundecanoic acid coated Au surfaces, in line with our results indicating that the lysine residues of site L, as well as K79 and K86 preferentially interact with the MPA-AuNP.

Figure 9. Degree of lysine modification determined by nanoLC-MS/MS. Site L (K22, K25, K27) exhibits a decrease in acetylation when incubated with MPA-AuNPs (red) compared to free cyt *c* (black) as do K86 of site A and K79. Site A exhibits an increase in labeling at lysines 73 and 74, as well as K5 and K39, upon incubation with MPA-AuNPs. Error bars represent the standard error of three independent experiments. Included spectral data had peptide identification with $p < 0.01$ and modification site identification with $p < 0.01$. Statistical analysis was performed with non-parametric one-way ANOVA ($\alpha = 0.05$; *** $p < 0.001$; ** $p < 0.01$; * $p < 0.05$).

Figure 10. Horse heart cyt *c* (1AKK). Lysines K5, K72, K73, and K39 had an increase in percent modification upon MPA-AuNP incubation (magenta). Lysines K22, K25, K27, K79, and K86 had a decrease in percent modification upon MPA-AuNP incubation (green). Lysines K7, K8, K60, K87, K88, K99, and K100 had no change in percent modification (cyan). Lysines K13, K60, and K53 were not detected by LC-MS/MS (gray).

Figure 11 summarizes the collective findings between the experiments and simulations. Two of the putative binding sites to cardiolipin, sites A and L, are seen to have some degree of preferred non-rigid binding to MPA-AuNP. Neither subspace of structures is perfectly aligned with the corresponding cardiolipin binding site because not all of a given site's residues are in proximity to MPA-AuNP at equilibrium. The poses that they take on are aligned, and exhibit similar orientation between simulation and experiment in so far as the lysine residues that are seen to be exposed or not exposed in the experiment are commensurate with the poses from the simulation. In these two orientations, the residues of sites A and L become less solvent accessible by either facing the MPA-AuNP surface or neighboring cyt *c* in the protein corona.

Figure 11. Two possible orientations of cyt *c* non-rigidly bound to MPA-AuNP consistent with the simulations and experiments are shown here: (a) K22 (in site L) and K86 and 87 (both in site A) facing the NP, and (b) K86 and K87 (both in site A) and K22 (in site L) facing the NP. In both orientations, K39 and K72 (in site A) are opposite to the MPA-AuNP and the most solvent accessible. K86 is closer to

the MPA-AuNP surface than K87, making it less solvent accessible, in agreement with footprinting experiments.

CONCLUSION

A central tenet of this work has been the advantages for combining experimental footprinting and computational molecular dynamics methods to efficiently converge on an optimal binding structure in long-lived hard coronas[63] even when binding is not fully specific or rigid. This was shown through the particular interaction between cyt *c* and 4 nm MPA-AuNPs, but the overall tandem strategy is general and represents a promising approach to quickly identify and verify potential binding regions. It can be used, for example, to probe preferential binding orientation and deformability of proteins in a NP size-dependent manner, as previously observed by simulations and experiments.[64-66] A key aspect to the success of the footprinting was the confirmation, suggested by the simulations, that lysine residues can be used as reporters for determining the possible poses of cyt *c* in relation to MPA-AuNP. Similarly, the results of the footprinting, in supporting the MD simulations, removed the need for determining a larger number of trajectories so as to reduce the error from the ensemble averaging of trajectories that would have come at large computational cost.

Previously, we observed a preferred binding site of cyt *c* on anionic lipid domains and the binding of MPA-AuNPs to membranes proportional to the number of cyt *c* on the membrane, using MD simulations and quartz crystal microbalance with dissipation monitoring experiments, respectively.[31] Through MD simulations and protein footprinting in this work, we show that cyt *c* can adopt two different but specific orientations in non-rigidly binding to MPA-AuNP. The solvent-exposed faces resulting from the preferred orientations of cyt *c* on membranes are thus available for cyt *c* to bind to MPA-AuNPs if that process is additive. Thus, protein footprinting

and MD simulations of peripheral membrane proteins adsorbed onto NPs provide a critical component to understand the role of cyt *c* in facilitating the binding of NPs to membranes. Given the technical challenges of exploring this three-way interaction, our ability to make these connections through pairwise studies is of particular significance. More generally, this combination of experimental and computational tools will find broad utility for the exploration of many pairwise and multi-component interactions to investigate mechanisms of protein corona formation and potentially, predict particle toxicity by the structure and reactivity of its corona.

MATERIALS AND METHODS

Materials. Gold(III) chloride trihydrate ($HAuCl_4$ $3H_2O$, ≥99.9%), 3-mercaptopropionic acid (99%), sodium borohydride ($NaBH_4$, >95%), cyt *c* from equine heart (BioUltra, ≥99% SDS-PAGE), *N*-hydroxysuccinimide (98%), acetic anhydride (ACS reagent, ≥98%), triethyl amine (NEt_3, ACS reagent grade), sodium hydroxide (ACS reagent), TRIS hydrochloride (ACS reagent, >99%), and tetrahydrofuran (THF, ACS reagent grade) were purchased from Millipore Sigma. Potassium cyanide (KCN, 99%) was purchased from Acros. All aqueous solutions were prepared with 18 MΩ MilliQ water. Glassware was cleaned prior to nanoparticle synthesis with aqua regia and rinsed thoroughly with MilliQ water.

Molecular Dynamics (MD) Simulations. To characterize the molecular interaction between cyt *c* (with structure 1AKK from the PDB)[67] and ligand-coated gold nanoparticles (AuNPs), several molecular dynamics (MD) simulations were performed with the two species in a large periodic box. The overall charge on the protein is +11.0, and the spatial charge distribution is shown in **Figure S1.1.** The AuNP model consisted of a fully atomistic, 4 nm gold core of 2123 atoms with fully deprotonated mercaptopropionic (MPA) acid ligands grafted uniformly on the AuNP surface,

following previous work,[68] at a ligand density of 5.6 molecules nm^{-2} as determined by experiment.[69] The CHARMM36 force field was used for protein-AuNP simulations.[70,71] Before the AuNPs and cyt *c* were combined into one simulation, we first performed separate equilibrations. The protein and AuNP were solvated in a TIP3P water box that provided an 8 Å padding between the molecules and the sides of the box. The solution was then neutralized and ionized using sodium and chloride ions to below physiological salt concentrations (0.01 M). These systems first underwent an energy minimization for 200,000 steps using the conjugate gradient algorithm. Thereafter, the system was equilibrated for 1 ns under NPT (constant pressure and temperature) conditions using a standard numerical barostat and thermostat as described below. For the protein system, backbone atoms as well as the iron and surrounding nitrogens on the heme group were held fixed during the process. Meanwhile, the gold atoms were similarly constrained for the nanoparticle's NPT equilibration. The final coordinates from these simulations were the initial conditions for 1.6 ns NVT (constant volume and temperature) equilibrations. During these relaxations, the previously imposed constraints on the atoms were gradually released. Specifically, a constraint with a 10 kcal mol^{-1} $Å^{-2}$ force constant was applied for the first 200 ps, followed by 200 ps with a 5 kcal mol^{-1} $Å^{-2}$ constraint, and then 200 ps with a 1 kcal mol^{-1} $Å^{-2}$ constraint. Finally, the system was allowed to equilibrate unconstrained for one 1 ns.

Once the protein and nanoparticle were equilibrated, the protein was placed in six different starting orientations with respect to the nanoparticle using PyMOL (**Figure S1.2**). By sampling all six of these orthogonally defined faces, we sampled the state space of possible orientations so as to obtain a statistically meaningful characterization of the relative preferred binding orientations. The center of mass of cyt *c* was held tangentially to the nanoparticle at a distance of approximately 30 Å, as shown in **Figures 2, 3, and S1.4**. This initial placement was intended to increase the amount of

protein surface area that is exposed to the nanoparticle, without overly biasing any particular binding site. The initial configurations were subsequently solvated with a 14 Å layer of TIP3P water. The nanoparticle and protein were placed along the longest diagonal of the simulation box with box volumes of approximately 1,000,000 $Å^3$ and average box length of 100 Å, which varied slightly depending on the dimensions of the protein configurations relative to the AuNP. These combined AuNP-cyt *c* systems were ionized and equilibrated using the same procedure as when they were equilibrated separately. After equilibration, 200 ns production runs with NVT conditions were used for data collection.

All simulations in this work were carried out using NAMD.[72] Particle Mesh Ewald (PME) with a 1.0 Å grid spacing was used to describe the electrostatics. Periodic boundary conditions and scaled 1-4 exclusions were also used throughout all simulations with a 12 Å pairwise-interaction cutoff and a switching function between 8 and 12 Å to address the nonbonded interactions. Additionally, all bonds were constrained using the SHAKE algorithm to allow for a 2 fs time step. Normally, long range electrostatics were only calculated every 10 fs, whereas short range nonbonded interactions were fully determined at every time step. However, when needed, the frequency of nonbonded force calculations was increased, or the time step was decreased, or both, during the equilibration steps to address errors within associated with the SHAKE algorithm.

Temperature was kept at a constant 300 K using a Langevin thermostat. It had a 5 ps^{-1} damping constant and was not coupled to hydrogens. For NPT steps, pressure was maintained at 1 atmosphere using a Langevin piston, with a period of 100 fs and decay rate of 50 fs. Under these conditions, the simulation box was allowed to expand isotropically in all dimensions. No Langevin piston was used for NVT simulations, and the dimensions of the box did not change.

MPA-AuNPs Synthesis. The MPA-AuNPs were synthesized by an adapted existing protocol as follows.[73] Briefly, 0.1 M $HAuCl_4$ (1.5 mL) was added to nanopure water (700 mL) in an Erlenmeyer flask followed by 0.1 M MPA (0.17 mL). The solution was adjusted to approximately pH 8.5 by the addition of 1 M NaOH solution, and stirred for 10 min. Then freshly made 0.1 M $NaBH_4$ (5 mL) was added, resulting in a rapidly color change to a deep red-brown. The reaction was stirred for 2 h at ambient temperature. The MPA-AuNPs were then concentrated by a customized flow reactor with a 50 kDa MWCO membrane (MilliporeSigma) to an approximate volume of 30 mL.[74] The concentrated MPA-AuNPs were then purified by diafiltration with 1 L of nanopure water *via* the flow reactor. The nanoparticles were characterized by UV-vis spectroscopy, transmission electron microscopy (TEM), dynamic light scattering measurement (DLS), and ζ-potential analysis. Complete characterization data is provided in the Supplemental Information.

Circular Dichroism. A solution of cyt *c* was prepared at 4 °C in MilliQ water at pH 8.6 (adjusted with 0.1 M NaOH). MPA-AuNPs were added for a final AuNP concentration of 18 nM and incubated overnight at 4 °C before measurements were taken, with the pH closely monitored. CD spectra were acquired on a JASCO J-815 Spectropolarimeter (JASCO Corporation, Tokyo, Japan) equipped with a temperature regulator. Approximately 250 µL of solution in 1 mm quartz cuvettes were measured at 20 °C, a bandwidth of 1.00 nm, a scanning speed of 50 nm/min, and baseline corrected to either a water blank for cyt *c* or an MPA-AuNP blank for cyt *c* and MPA-AuNP conjugates. The CD traces shown are an average of 10 scans, which were smoothed with a Gaussian-weighted moving average filter (MATLAB and Statistics Toolbox R2018a). The percent composition of secondary structures was calculated from the CD spectra using the CONTIN program in CDPro.[54]

Lysine-Specific Protein Footprinting. Lyophilized horse heart cyt *c* (10.0 mg) was dissolved in MilliQ water (1.00 mL). This stock was stored at –20 °C. Concentrations of cyt *c* at pH 8.6 in H_2O were confirmed by UV-Vis spectroscopy at 408 nm (extinction coefficient 106,000 M^{-1} cm^{-1}). A cyt *c* solution of 100 nM was prepared in a 500 mL volumetric flask (704 μL of 71 μM cyt *c* stock) and the pH was adjusted to 8.6 with 0.1 M NaOH. To a 250 mL volumetric flask was added MPA-coated AuNPs (4.31 mL of 580 nM) and the 100 nM cyt *c* solution was used to bring the volume to 250 mL. The resulting solution was 10 nM MPA-coated AuNPs and 100 nM in cyt *c*, for a protein:NP ratio of 10:1. The solutions were allowed to equilibrate overnight at ambient temperature. Immediately before the lysine acetylation reaction, the pH was checked to ensure it remained at 8.6.

The free 100 nM cyt *c* and 10 nM AuNP incubated 100 nM cyt *c* were split into 10 mL aliquots in 50 mL Falcon tubes. To each reaction was added 60 mM *N*-acetoxy succinimide (166 μL, 10 μmol, 10,000 equiv.). The reaction was gently swirled and allowed to react for 1 min at ambient temperature. Then 60 mM Tris (166 μL, 10 μmol, 10,000 equiv.) was added to quench unreacted *N*-acetoxy-succinimide.

The AuNPs were dissolved according to an altered procedure by Lee and co-workers.[75] To the crude mixture of both free cyt *c* and AuNP incubated cyt *c* was added 0.4 M KCN (1.0 mL). KCN should not affect cyt *c* for mass spectrometry analysis; however, free cyt *c* samples were also treated with KCN to ensure identical sample preparation. **Important safety note:** Only work with KCN in a ventilation hood and ensure solutions remain at a basic pH to avoid formation of toxic HCN gas. The mixtures were incubated at 60 °C for 10 min, during which time the AuNP solution turned clear. Cyt *c* was then recovered by using a 10 kDA MWCO filter (Millipore Sigma) at 8,000

rpm and then evaporated to dryness (Eppendorf Vacufuge Plus). Cyt *c* was reconstituted in 10 mM ammonium bicarbonate buffer (pH 7.4) and denatured at 95 °C for 15 mins. Cyt *c* was then digested by chymotrypsin at 37 °C overnight in a 1:40 chymotrypsin/ cyt *c* ratio. The digestion was stopped by addition of 20 μL 10% TFA and the peptides were evaporated to dryness *in vacuo*. The samples were prepared for LC-MS/MS analysis with C18 ZipTips (Millipore) according to manufacturer's specifications.

NanoLC-MS/MS Analysis. LC-MS/MS was performed on a Thermo Scientific Orbitrap Elite and a Luna C18 column (Phenomenex; 75 μm inner diameter, 20 cm length, 100 Å pore size). All MS measurements were performed in the positive ion mode *via* higher-energy collisional dissociation (HCD). Precursor ions were measured at a resolution of 60,000 in the Orbitrap analyzer. The top ten most intense ions from each MS scan were chosen for isolation, fragmentation, and detection. Biological triplicates were analyzed with three nanoLC-MS/MS analyses, with the exception of one biological set of cyt *c* bound to MPA-AuNP, which was analyzed twice by nanoLC-MS/MS as the third run did not have sufficient signal.

Peptide Identification and Percent Modification. Peptide identification and percent modification were carried out with PEAKS 8.5 software (BioInformatics Software Inc.). The data were searched against the UniProt database. Variable lysine acetylations (+42.01 *m*/*z*) were set as modifications and chymotrypsin digestion specificity was set for two missed cleavage sites. On average, 95% sequence coverage for cyt *c* was observed for all samples. Full search parameters are included in the Supplemental Information. For percent modification calculations, only peptides with a p value ≤ 0.01 and residue modification assignments with a p value ≤ 0.01 were included in the calculations to ensure confidence in assignment. Statistical analysis of the data was

performed with non-parametric one-way ANOVA ($\alpha = 0.05$; ***$p < 0.001$; **$p < 0.01$; *$p < 0.05$). Peptide and residue modification assignments for three lysines (K13, K53, and K60) did not meet the statistical parameters for confident identification and were not reported.

TOC Graphic

ASSOCIATED CONTENT

Supporting Information. Results from simulations of free cyt *c* in TIP3P solvent and simulations of MPA-AuNP with the other initial orientations of cyt *c* not presented here in the main text. Additional methods and results for the synthesis and characterization of MPA-AuNPs and characterization of cyt *c* adsorption onto MPA-AuNPs. This material is available free of charge *via* the Internet at http://pubs.acs.org.

The authors declare no competing financial interests.

AUTHOR INFORMATION

Corresponding Authors

*E-mail: r.hernandez@jhu.edu; carlsone@umn.edu

Author contributions: R.H., E.E.C., C.J.M., J.A.P. conceived the study; C.A. conducted molecular dynamics simulations; E.J.T and J.J.C conducted CD and mass spectrometry experiments; X.Z. synthesized and characterized the nanoparticles; E.J.T., C.A., G.C., X.Z., E.E.C., R.H. analyzed data; E.J.T., C.A., G.C., J.A.P., C.J.M, E.E.C., R.H. wrote the paper.

ACKNOWLEDGMENTS

This work was supported by the National Science Foundation (NSF) under the Center for Sustainable Nanotechnology (CHE-1503408). The computing resources necessary for this research were provided in part by the NSF through XSEDE resources provided by Comet (TG-CTS090079), and by the Maryland Advanced Research Computing Center (MARCC). E.J.T. would like to thank Dr. LeeAnn Higgins, Todd Markowski and Dr. Yingchun Zhao for assistance with mass spectrometry and Mike Fealey for assistance with CD analysis.

REFERENCES

1. Murphy, C. J.; Gole, A. M.; Stone, J. W.; Sisco, P. N.; Alkilany, A. M.; Goldsmith, E. C.; Baxter, S. C. Gold Nanoparticles in Biology: Beyond Toxicity to Cellular Imaging. *Acc. Chem. Res.* **2008,** *41*, 1721-1730.
2. Shemetov, A. A.; Nabiev, I.; Sukhanova, A. Molecular Interaction of Proteins and Peptides with Nanoparticles. *ACS Nano* **2012,** *6*, 4585-4602.
3. Murphy, C. J.; Vartanian, A. M.; Geiger, F. M.; Hamers, R. J.; Pedersen, J. A.; Cui, Q.; Haynes, C. L.; Carlson, E. E.; Hernandez, R.; Klaper, R. D.; Orr, G.; Rosenzweig, Z. Biological Responses to Engineered Nanomaterials: Needs for the Next Decade. *ACS Cent. Sci.* **2015,** *1*, 117–123.
4. Cui, Q.; Hernandez, R.; Mason, S. E.; Frauenheim, T.; Pedersen, J. A.; Geiger, F. Sustainable Nanotechnology: Opportunities and Challenges for Theoretical/Computational Studies. *Journal of Physical Chemistry B* **2016,** *120*, 7297-7306.
5. Carrillo-Carrion, C.; Carril, M.; Parak, W. J. Techniques for the Experimental Investigation of the Protein Corona. *Curr. Opin. Biotechnol.* **2017,** *46*, 106-113.
6. Mahmoudi, M.; Lynch, I.; Ejtehadi, M. R.; Monopoli, M. P.; Bombelli, F. B.; Laurent, S. Protein−Nanoparticle Interactions: Opportunities and Challenges. *Chem. Rev.* **2011,** *111*, 5610-5637.
7. Brewer, S. H.; Glomm, W. R.; Johnson, M. C.; Knag, M. K.; Franzen, S. Probing BSA Binding to Citrate-Coated Gold Nanoparticles and Surfaces. *Langmuir* **2005,** *21*, 9303-9307.
8. Lacerda, S. H. D. P.; Park, J. J.; Meuse, C.; Pristinski, D.; Becker, M. L.; Karim, A.; Douglas, J. F. Interaction of Gold Nanoparticles with Common Human Blood Proteins. *ACS Nano* **2010,** *4*, 365-379.
9. Casals, E.; Pfaller, T.; Duschl, A.; Oostingh, G. J.; Puntes, V. Time Evolution of the Nanoparticle Protein Corona. *ACS Nano* **2010,** *4*, 3623-3632.

10. Maiorano, G.; Sabella, S.; Sorce, B.; Brunetti, V.; Malvindi, M. A.; Cingolani, R.; Pompa, P. P. Effects of Cell Culture Media on the Dynamic Formation of Protein-Nanoparticle Complexes and Influence on the Cellular Response. *ACS Nano* **2010,** *4*, 7481-7491.
11. Melby, E. S.; Lohse, S. E.; Park, J. E.; Vartanian, A. M.; Putans, R. A.; Abbott, H. B.; Hamers, R. J.; Murphy, C. J.; Pedersen, J. A. Cascading Effects of Nanoparticle Coatings: Surface Functionalization Dictates the Assemblage of Complexed Proteins and Subsequent Interaction with Model Cell Membranes. *ACS Nano* **2017,** *11*, 5489-5499.
12. Bortot, A.; Zanzoni, S.; D'Onofrio, M.; Assfalg, M. Specific Interaction Sites Determine Differential Adsorption of Protein Structural Isomers on Nanoparticle Surfaces. *Chem. Eur. J.* **2018,** *24*, 5911-5919.
13. Li, N.; Zeng, S.; He, L.; Zhong, W. Exploration of Possible Binding Sites of Nanoparticles on Protein by Cross-Linking Chemistry Coupled with Mass Spectrometry. *Anal. Chem.* **2011,** *83*, 6929-6934.
14. Mendoza, V. L.; Vachet, R. W. Probing Protein Structure by Amino Acid-Specific Covalent Labeling and Mass Spectrometry. *Mass Spectrom. Rev.* **2009,** *28*, 785-815.
15. Wang, L.; Chance, M. R. Protein Footprinting Comes of Age: Mass Spectrometry for Biophysical Structure Assessment. *Mol. Cell. Proteomics* **2017,** *16*, 706-716.
16. Shrivastava, S.; McCallum, S. A.; Nuffer, J. H.; Qian, X.; Siegel, R. W.; Dordick, J. S. Identifying Specific Protein Residues That Guide Surface Interactions and Orientation on Silica Nanoparticles. *Langmuir* **2013,** *29*, 10841-10849.
17. Shrivastava, S.; Nuffer, J. H.; Siegel, R. W.; Dordick, J. S. Position-Specific Chemical Modification and Quantitative Proteomics Disclose Protein Orientation Adsorbed on Silica Nanoparticles. *Nano Lett.* **2012,** *12*, 1583-1587.
18. Bayraktar, H.; You, C.-C.; Rotello, V. M.; Knapp, M. J. Facial Control of Nanoparticle Binding to Cytochrome c. *J. Am. Chem. Soc.* **2007,** *129*, 2732-2733.
19. Devineau, S.; Mathé, C.; Legros, V.; Gonnet, F.; Daniel, R.; Renault, J. P.; Pin, S. The Nano-Bio Interface Mapped by Oxidative Footprinting of the Adsorption Sites of Myoglobin. *Anal. Bioanal. Chem.* **2014,** *406*, 8037-8040.
20. Shao, Q.; Hall, C. K. Protein Adsorption on Nanoparticles: Model Development Using Computer Simulation. *J. Phys.: Condens. Matter* **2016,** *28*, 414019.
21. Tavanti, F.; Pedone, A.; Menziani, M. C. Competitive Binding of Proteins to Gold Nanoparticles Disclosed by Molecular Dynamics Simulations. *J. Phys. Chem. C* **2015,** *119*, 22172-22180.
22. Smith, J.; Sprenger, K. G.; Liao, R.; Joseph, A.; Nance, E.; Pfaendtner, J. Determining Dominant Driving Forces Affecting Controlled Protein Release from Polymeric Nanoparticles. *Biointerphases* **2017,** *12*.
23. Brancolini, G.; Tozzini, V. Multiscale Modeling of Proteins Interaction with Functionalized Nanoparticles. *Curr. Opin. Colloid Interface Sci.* **2019,** *41*, 66-73.
24. Ghorai, P. K.; Glotzer, S. C. Molecular Dynamics Simulation Study of Self-Assembled Monolayers of Alkanethiol Surfactants on Spherical Gold Nanoparticles. *J. Phys. Chem. C* **2007,** *111*, 15857-15862.
25. Brancolini, G.; Corazza, A.; Vuano, M.; Fogolari, F.; Mimmi, M. C.; Bellotti, V.; Stoppini, M.; Corni, S.; Esposito, G. Probing the Influence of Citrate-Capped Gold Nanoparticles on an Amyloidogenic Protein. *ACS Nano* **2015,** *9*, 2600-2613.

26. Lin, W.; Insley, T.; Tuttle, M. D.; Zhu, L. Y.; Berthold, D. A.; Kral, P.; Rienstra, C. M.; Murphy, C. J. Control of Protein Orientation on Gold Nanoparticles. *J. Phys. Chem. C* **2015,** *119*, 21035-21043.
27. Chong, G.; Laudadio, E. D.; Wu, M.; Murphy, C. J.; Hamers, R. J.; Hernandez, R. Density, Structure, and Stability of $Citrate^{3-}$ and $H_2citrate^-$ on Bare and Coated Gold Nanoparticles. *J. Phys. Chem. C* **2018,** *122*, 28393-28404.
28. Reed, J. C. Cytochrome c: Can't Live with It - Can't Live without It. *Cell* **1997,** *91*, 559-562.
29. Tuominen, E. K.; Wallace, C. J.; Kinnunen, P. K. Phospholipid-Cytochrome c Interaction: Evidence for the Extended Lipid Anchorage. *J. Biol. Chem.* **2002,** *277*, 8822-6.
30. Kalanxhi, E.; Wallace, C. J. Cytochrome c Impaled: Investigation of the Extended Lipid Anchorage of a Soluble Protein to Mitochondrial Membrane Models. *Biochem. J.* **2007,** *407*, 179-87.
31. Melby, E. S.; Allen, C.; Foreman-Ortiz, I.; Caudill, E.; Kuech, T. R.; Vartanian, A. M.; Zhang, X.; Murphy, C. J.; Hernandez, R.; Pedersen, J. A. Peripheral Membrane Proteins Facilitate Nanoparticle Binding at Lipid Bilayer Interfaces. *Langmuir* **2018,** *34*, 10793–10805.
32. Troiano, J. M.; Olenick, L. L.; Kuech, T. R.; Melby, E. S.; Hu, D.; Lohse, S. E.; Mensch, A. C.; Dogangun, M.; Vartanian, A. M.; Torelli, M. D.; Ehimiaghe, E.; Walter, S. R.; Fu, L.; Anderton, C. R.; Zhu, Z.; Wang, H.; Orr, G.; Murphy, C. J.; Hamers, R. J.; Pedersen, J. A.*, et al.* Direct Probes of 4 nm Diameter Gold Nanoparticles Interacting with Supported Lipid Bilayers. *J. Phys. Chem. C* **2015,** *119*, 534-546.
33. Rytömaa, M.; Kinnunen, P. K. J. Evidence for Two Distinct Acidic Phospholipid-Binding Sites in Cytochrome c. *J. Biol. Chem.* **1994,** *269*, 1770-1774.
34. Rytömaa, M.; Kinnunen, P. K. J. Reversibility of the Binding of Cytochrome c to Liposomes: Implications for Lipid-Protein Interactions. *J. Biol. Chem.* **1995,** *270*, 3197-3202.
35. Elmer-Dixon, M. M.; Bowler, B. E. Electrostatic Constituents of the Interaction of Cardiolipin with Site A of Cytochrome c. *Biochemistry* **2018,** *57*, 5683-5695.
36. Walczyk, D.; Bombelli, F. B.; Monopoli, M. P.; Lynch, I.; Dawson, K. A. What the Cell "Sees" in Bionanoscience. *J. Am. Chem. Soc.* **2010,** *132*, 5762-5768.
37. Casals, E.; Pfaller, T.; Duschl, A.; Oostingh, G. J.; Puntes, V. F. Hardening of the Nanoparticle-Protein Corona in Metal (Au, Ag) and Oxide (Fe_3O_4, CoO, and CeO_2) Nanoparticles. *Small* **2011,** *7*, 3479-3486.
38. Wang, A. L.; Perera, Y. R.; Davidson, M. B.; Fitzkee, N. C. Electrostatic Interactions and Protein Competition Reveal a Dynamic Surface in Gold Nanoparticle-Protein Adsorption. *J. Phys. Chem. C* **2016,** *120*, 24231-24239.
39. O'Brien, E. S.; Nucci, N. V.; Fuglestad, B.; Tommos, C.; Wand, A. J. Defining the Apoptotic Trigger: The Interaction of Cytochrome c and Cardiolipin. *J. Biol. Chem.* **2015,** *290*, 30879-30887.
40. Kawai, C.; Prado, F. M.; Nunes, G. L.; Di Mascio, P.; Carmona-Ribeiro, A. M.; Nantes, I. L. pH-Dependent Interaction of Cytochrome c with Mitochondrial Mimetic Membranes: The Role of an Array of Positively Charged Amino Acids. *J. Biol. Chem.* **2005,** *280*, 34709-34717.
41. Sinibaldi, F.; Howes, B. D.; Droghetti, E.; Polticelli, F.; Piro, M. C.; Di Pierro, D.; Fiorucci, L.; Coletta, M.; Smulevich, G.; Santucci, R. Role of Lysines in Cytochrome c-Cardiolipin Interaction. *Biochemistry* **2013,** *52*, 4578-4588.

42. Kinnunen, P. K. J.; Koiv, A.; Lehtonen, J. Y. A.; Rytomaa, M.; Mustonen, P. Lipid Dynamics and Peripheral Interactions of Proteins with Membrane Surfaces. *Chem. Phys. Lipids* **1994,** *73*, 181-207.
43. Tavanti, F.; Pedone, A.; Matteini, P.; Menziani, M. C. Computational Insight into the Interaction of Cytochrome C with Wet and PVP-Coated Ag Surfaces. *J. Phys. Chem. B* **2017,** *121*, 9532-9540.
44. Kataoka, M.; Hagihara, Y.; Mihara, K.; Goto, Y. Molten Globule of Cytochrome-C Studied by Small-Angle X-Ray-Scattering. *J. Mol. Biol.* **1993,** *229*, 591-596.
45. Greenfield, N. J. Using Circular Dichroism Spectra to Estimate Protein Secondary Structure. *Nat. Protoc.* **2007,** *1*, 2876-2890.
46. Kelly, S. M.; Jess, T. J.; Price, N. C. How to Study Proteins by Circular Dichroism. *Biochim. Biophys. Acta, Proteins Proteomics* **2005,** *1751*, 119-139.
47. Barrow, C. J.; Yasuda, A.; Kenny, P. T. M.; Zagorski, M. G. Solution Conformations and Aggregational Properties of Synthetic Amyloid β-Peptides of Alzheimer's Disease: Analysis of Circular Dichroism Spectra. *J. Mol. Biol.* **1992,** *225*, 1075-1093.
48. Wallimann, P.; Kennedy, R. J.; Miller, J. S.; Shalongo, W.; Kemp, D. S. Dual Wavelength Parametric Test of Two-State Models for Circular Dichroism Spectra of Helical Polypeptides: Anomalous Dichroic Properties of Alanine-Rich Peptides. *J. Am. Chem. Soc.* **2003,** *125*, 1203-1220.
49. Valušová, E.; Švec, P.; Antalík, M. Structural and Thermodynamic Behavior of Cytochrome c Assembled with Glutathione-Covered Gold Nanoparticles. *J. Biol. Inorg. Chem.* **2009,** *14*, 621.
50. Shang, W.; Nuffer, J. H.; Muñiz-Papandrea, V. A.; Colón, W.; Siegel, R. W.; Dordick, J. S. Cytochrome c on Silica Nanoparticles: Influence of Nanoparticle Size on Protein Structure, Stability, and Activity. *Small* **2009,** *5*, 470-476.
51. Aubin-Tam, M.-E.; Hamad-Schifferli, K. Gold Nanoparticle−Cytochrome c Complexes: The Effect of Nanoparticle Ligand Charge on Protein Structure. *Langmuir* **2005,** *21*, 12080-12084.
52. Jiang, X.; Jiang, J.; Jin, Y.; Wang, E.; Dong, S. Effect of Colloidal Gold Size on the Conformational Changes of Adsorbed Cytochrome c: Probing by Circular Dichroism, UV−Visible, and Infrared Spectroscopy. *Biomacromolecules* **2005,** *6*, 46-53.
53. Zhao, H.-Z.; Du, Q.; Li, Z.-S.; Yang, Q.-Z. Mechanisms for the Direct Electron Transfer of Cytochrome c Induced by Multi-Walled Carbon Nanotubes. *Sensors* **2012,** *12*, 10450.
54. Sreerama, N.; Woody, R. W. Estimation of Protein Secondary Structure from Circular Dichroism Spectra: Comparison of CONTIN, SELCON, and CDSSTR Methods with an Expanded Reference Set. *Anal. Biochem.* **2000,** *287*, 252-260.
55. Balakrishnan, G.; Hu, Y.; Spiro, T. G. His26 Protonation in Cytochrome c Triggers Microsecond β-sheet Formation and Heme Exposure: Implications for Apoptosis. *J. Am. Chem. Soc.* **2012,** *134*, 19061-19069.
56. Novak, P.; Kruppa, G. H.; Young, M. M.; Schoeniger, J. A Top-Down Method for the Determination of Residue-Specific Solvent Accessibility in Proteins. *J. Mass Spectrom.* **2004,** *39*, 322-328.
57. Marini, M. A.; Marti, G. E.; Berger, R. L.; Martin, C. J. Potentiometric Titration Curves of Oxidized and Reduced Horse Heart Cytochrome c. *Biopolymers* **1980,** *19*, 885-898.
58. Bos, M. A.; Kleijn, J. M. Determination of the Orientation Distribution of Adsorbed Fluorophores Using TIRF. II. Measurements on Porphyrin and Cytochrome c. *Biophys. J.* **1995,** *68*, 2573-2579.

59. Dennison, J. M.; Zupancic, J. M.; Lin, W.; Dwyer, J. H.; Murphy, C. J. Protein Adsorption to Charged Gold Nanospheres as a Function of Protein Deformability. *Langmuir* **2017,** *33*, 7751-7761.
60. Ahmad, R.; Jang, H.; Batule, B. S.; Park, H. G. Barcode DNA-Mediated Signal Amplifying Strategy for Ultrasensitive Biomolecular Detection on Matrix-Assisted Laser Desorption Ionization Time of Flight (MALDI-TOF) Mass Spectrometry. *Anal. Chem.* **2017,** *89*, 8966-8973.
61. Han, X.; He, L.; Xin, L.; Shan, B.; Ma, B. PeaksPTM: Mass Spectrometry-Based Identification of Peptides with Unspecified Modifications. *J. Proteome Res.* **2011,** *10*, 2930-2936.
62. Nakano, K.; Yoshitake, T.; Yamashita, Y.; Bowden, E. F. Cytochrome c Self-Assembly on Alkanethiol Monolayer Electrodes as Characterized by AFM, IR, QCM, and Direct Electrochemistry. *Langmuir* **2007,** *23*, 6270-6275.
63. Loftus, A. F.; Reighard, K. P.; Kapourales, S. A.; Leopold, M. C. Monolayer-Protected Nanoparticle Film Assemblies as Platforms for Controlling Interfacial and Adsorption Properties in Protein Monolayer Electrochemistry. *J. Am. Chem. Soc.* **2008,** *130*, 1649-1661.
64. Tavanti, F.; Pedone, A.; Menziani, M. C. A Closer Look into the Ubiquitin Corona on Gold Nanoparticles by Computational Studies. *New J. Chem.* **2015,** *39*, 2474-2482.
65. Wei, S.; Ahlstrom, L. S.; Brooks III, C. L. Exploring Protein-Nanoparticle Interactions with Coarse-Grained Protein Folding Models. *Small* **2017,** *13*.
66. Woods, K. E.; Perera, Y. R.; Davidson, M. B.; Wilks, C. A.; Yadav, D. K.; Fitzkee, N. C. Understanding Protein Structure Deformation on the Surface of Gold Nanoparticles of Varying Size. *J. Phys. Chem. C* **2016,** *120*, 27944-27953.
67. Banci, L.; Bertini, I.; Gray, H. B.; Luchinat, C.; Reddig, T.; Rosato, A.; Turano, P. Solution Structure of Oxidized Horse Heart Cytochrome c. *Biochemistry* **1997,** *36*, 9867-9877.
68. Wu, M.; Vartanian, A. M.; Chong, G.; Pandiakumar, A. K.; Hamers, R. J.; Hernandez, R.; Murphy, C. J. Solution NMR Analysis of Ligand Environment in Quaternary Ammonium-Terminated Self-Assembled Monolayers on Gold Nanoparticles: The Effect of Surface Curvature and Ligand Structure. *J. Am. Chem. Soc.* **2019,** *141*, 4316-4327.
69. Feng, Z. V.; Gunsolus, I. L.; Qiu, T. A.; Hurley, K. R.; Nyberg, L. H.; Frew, H.; Johnson, K. P.; Vartanian, A. M.; Jacob, L. M.; Lohse, S. E.; Torelli, M. D.; Hamers, R. J.; Murphy, C. J.; Haynes, C. L. Impacts of Gold Nanoparticle Charge and Ligand Type on Surface Binding and Toxicity to Gram-Negative and Gram-Positive Bacteria. *Chem. Sci.* **2015,** *6*, 5186-5196.
70. Best, R. B.; Zhu, X.; Shim, J.; Lopes, P. E.; Mittal, J.; Feig, M.; Mackerell, A. D., Jr. Optimization of the Additive CHARMM All-Atom Protein Force Field Targeting Improved Sampling of the Backbone Phi, Psi and Side-Chain Chi(1) and Chi(2) Dihedral Angles. *J. Chem. Theory Comput.* **2012,** *8*, 3257-3273.
71. Huang, J.; Mackerell, A. D., Jr. CHARMM36 All-Atom Additive Protein Force Field: Validation Based on Comparison to NMR Data. *J. Comput. Chem.* **2013,** *34*, 2135-2145.
72. Kalé, L.; Skeel, R.; Bhandarkar, M.; Brunner, R.; Gursoy, A.; Krawetz, N.; Phillips, J.; Shinozaki, A.; Varadarajan, K.; Schulten, K. NAMD2: Greater Scalability for Parallel Molecular Dynamics. *J. Comput. Phys.* **1999,** *151*, 283-312.
73. Bozich, J. S.; Lohse, S. E.; Torelli, M. D.; Murphy, C. J.; Hamers, R. J.; Klaper, R. D. Surface Chemistry, Charge and Ligand Type Impact the Toxicity of Gold Nanoparticles to *Daphnia magna*. *Environ. Sci.: Nano* **2014,** *1*, 260-270.
74. Lohse, S. E.; Eller, J. R.; Sivapalan, S. T.; Plews, M. R.; Murphy, C. J. A Simple Millifluidic Benchtop Reactor System for the High-Throughput Synthesis and Functionalization of Gold Nanoparticles with Different Sizes and Shapes. *ACS Nano* **2013,** *7*, 4135-4150.

75. Lee, H.; Park, J.-E.; Nam, J.-M. Bio-Barcode Gel Assay for microRNA. *Nat. Commun.* **2014,** *5*.

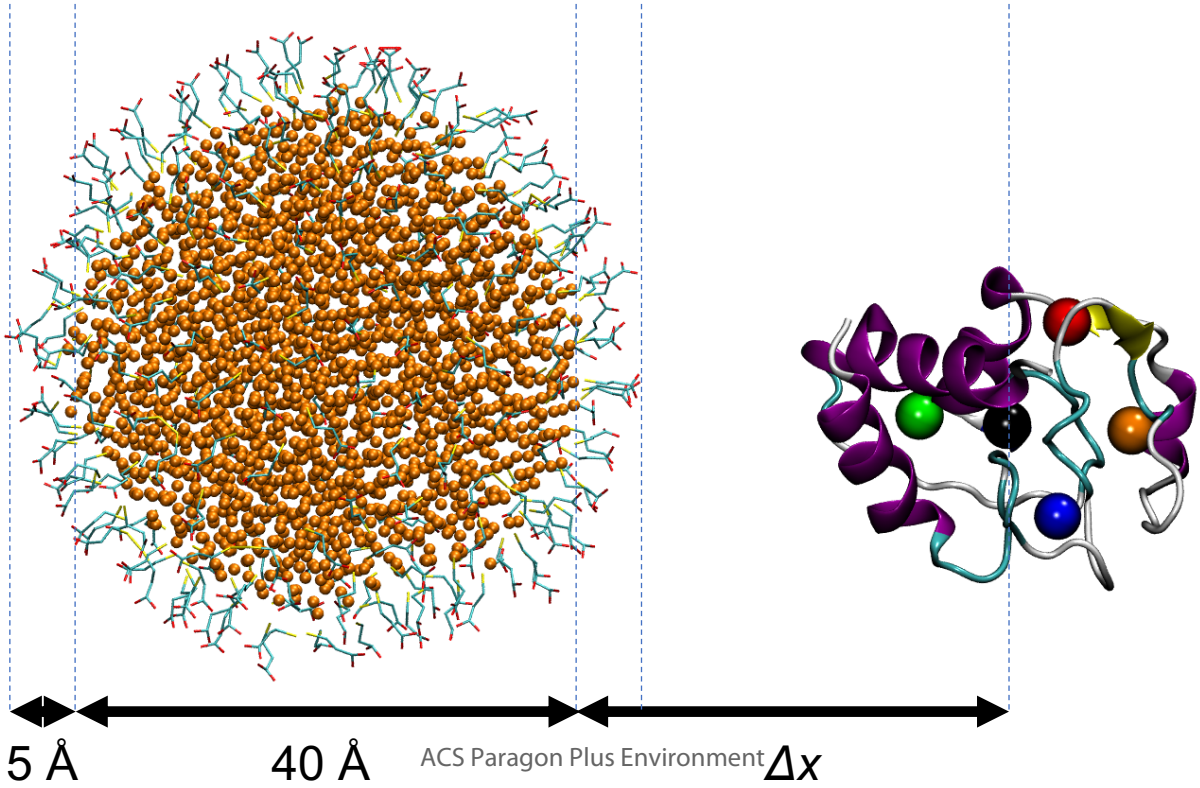
5 Å
40 Å
ACS Paragon Plus Environment
Δx

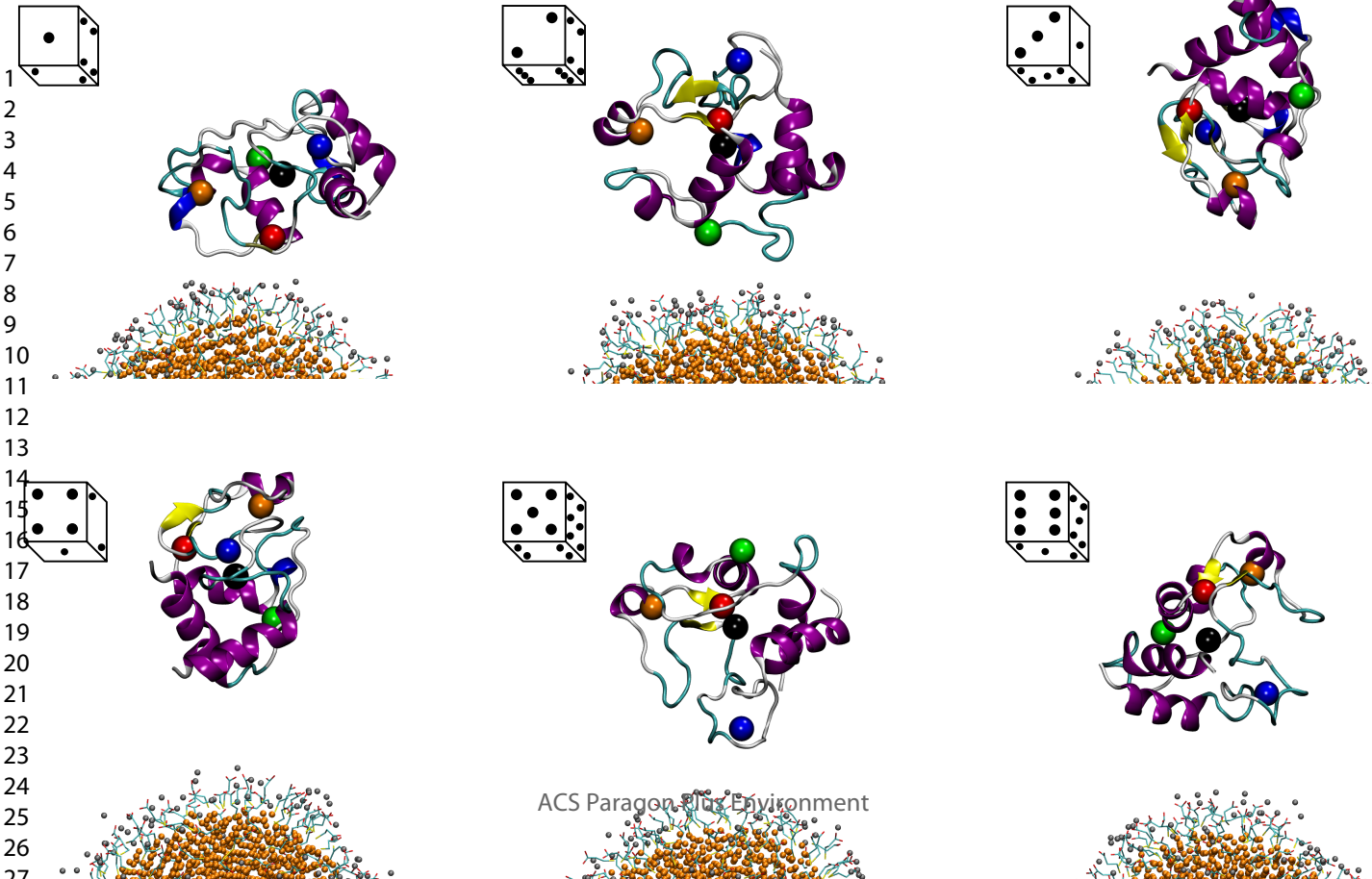

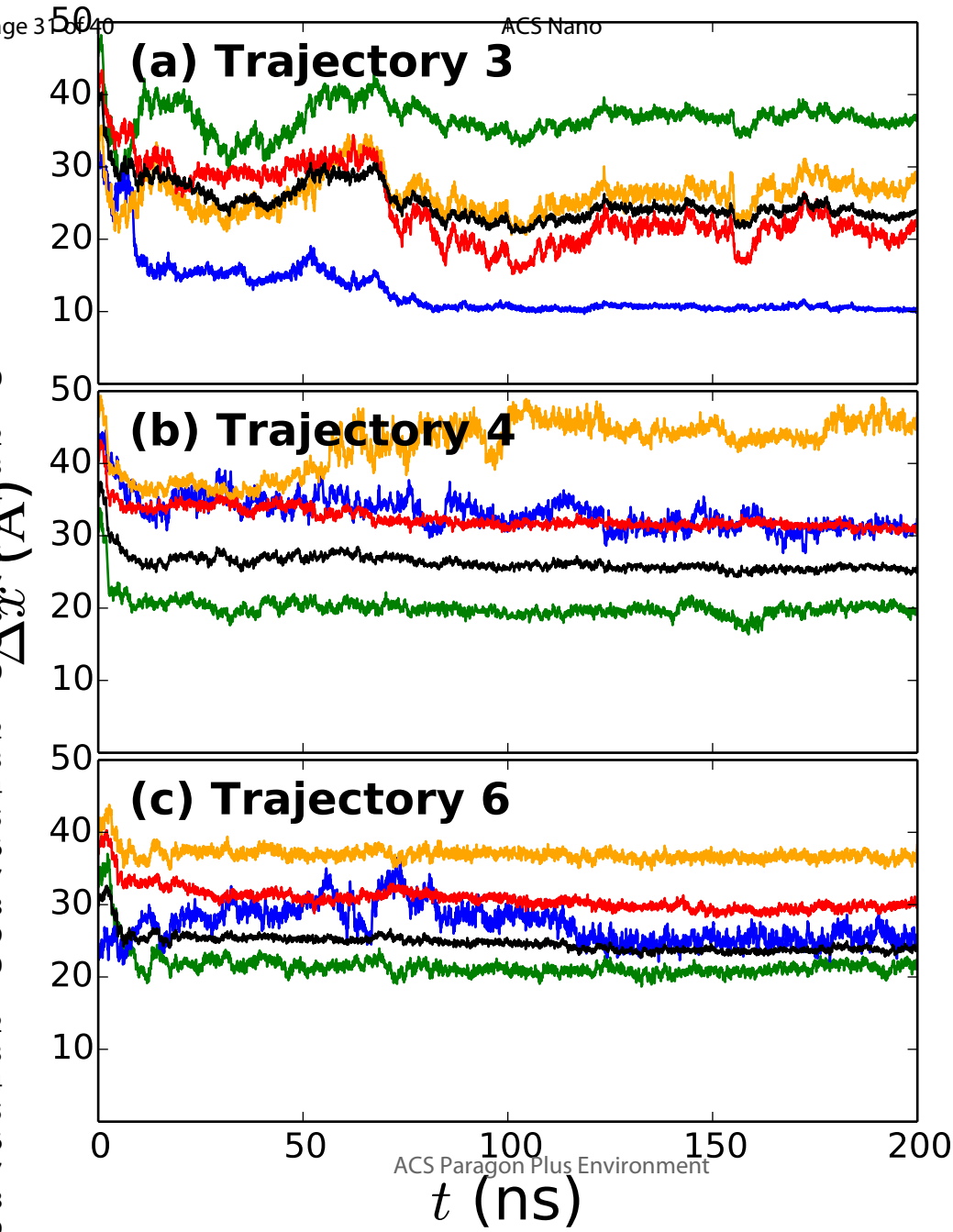
(a) Trajectory 3
(b) Trajectory 4
(c) Trajectory 6
Site A
Site L
Site C
Site N
Cyt c
Δx (Å)
t (ns)
0
50
100
150
200
10
20
30
40
50

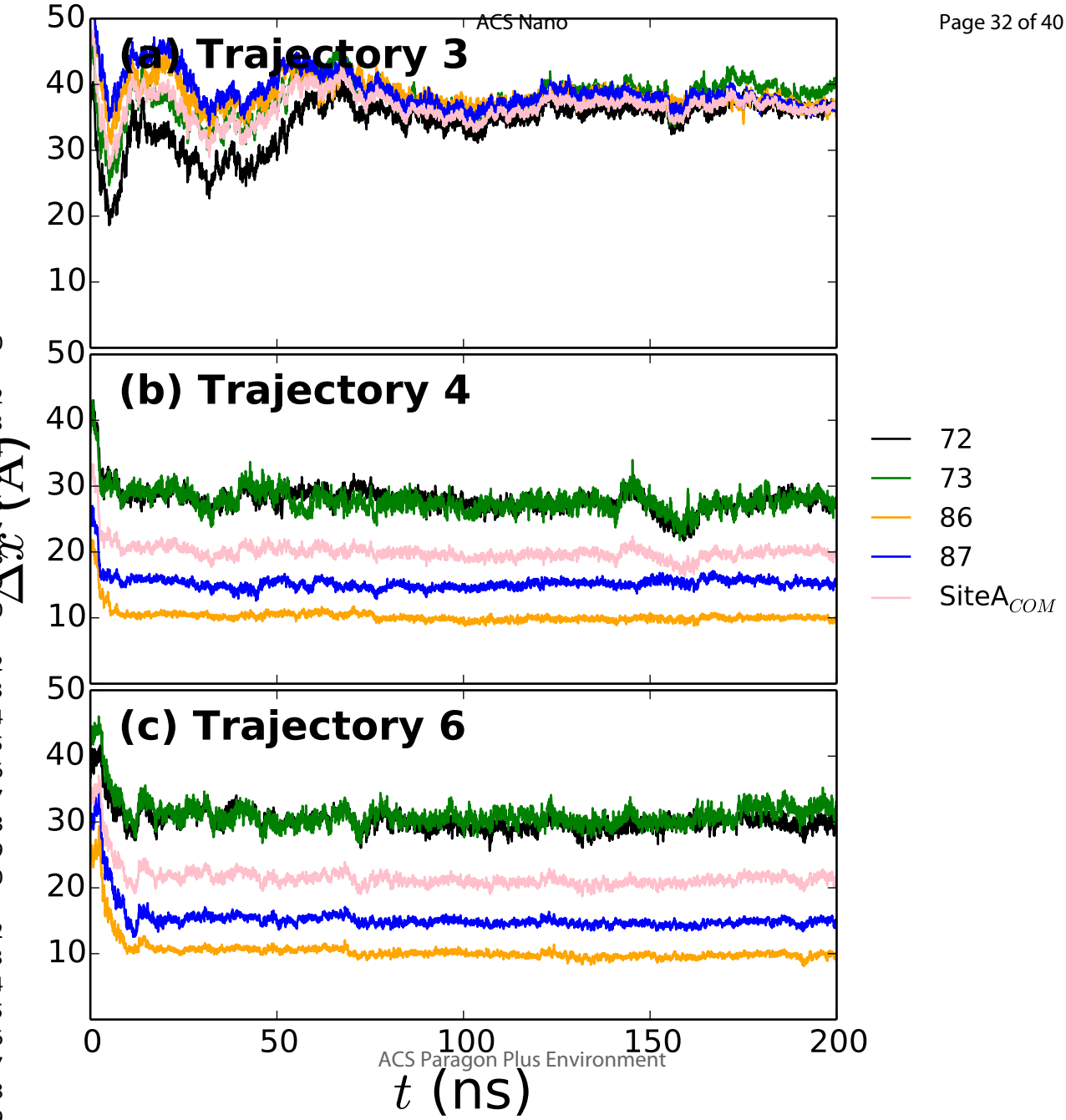
(a) Trajectory 3
(b) Trajectory 4
(c) Trajectory 6
Δx (Å)
t (ns)
0
50
100
150
200
10
20
30
40
50
72
73
86
87
SiteA$_{COM}$

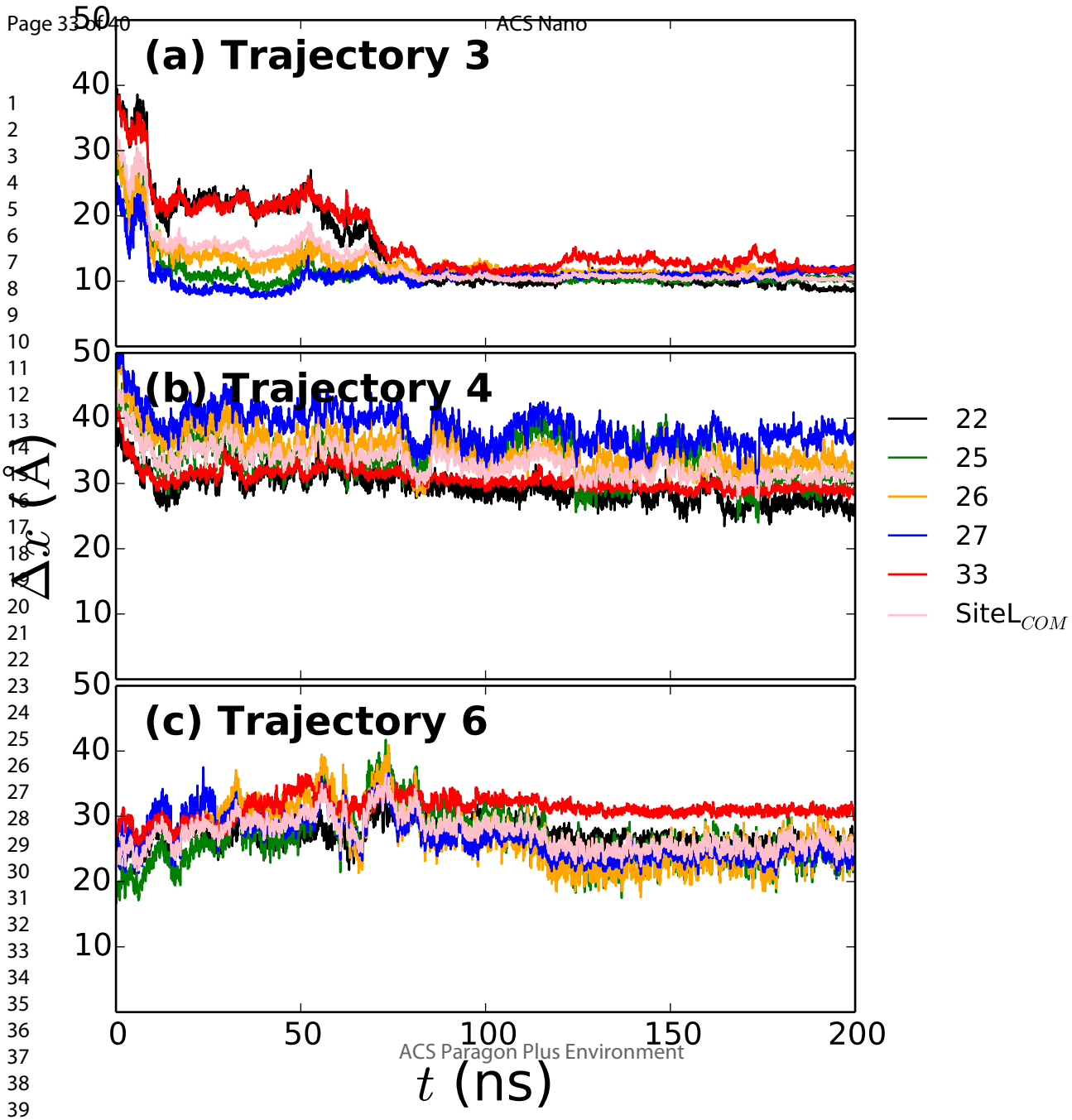
(a) Trajectory 3
(b) Trajectory 4
(c) Trajectory 6
Δx (Å)
t (ns)
22
25
26
27
33
SiteL$_{COM}$

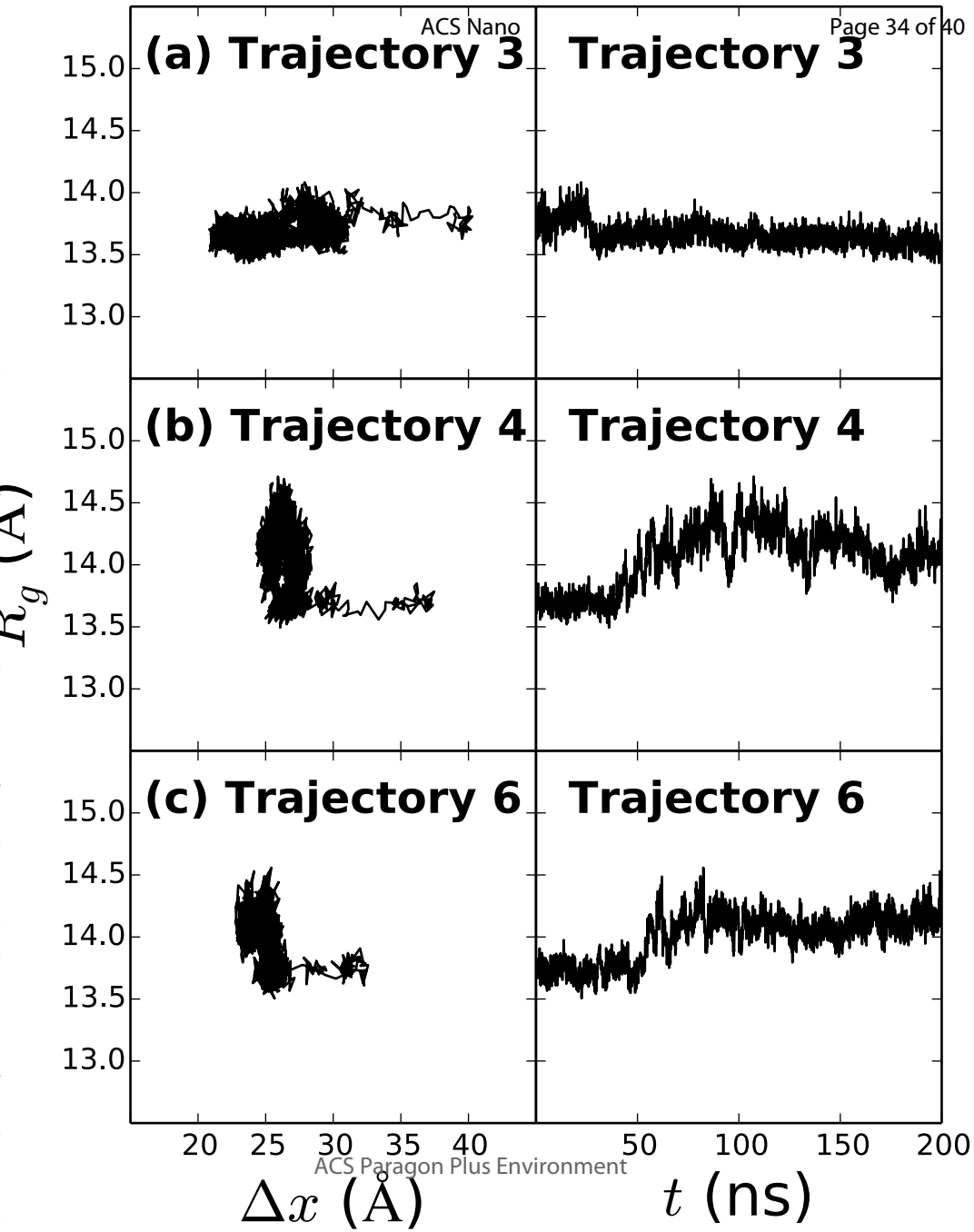
(a) Trajectory 3
Trajectory 3
(b) Trajectory 4
Trajectory 4
(c) Trajectory 6
Trajectory 6
15.0
14.5
14.0
13.5
13.0
R_g (Å)
20
25
30
35
40
Δx (Å)
50
100
150
200
t (ns)

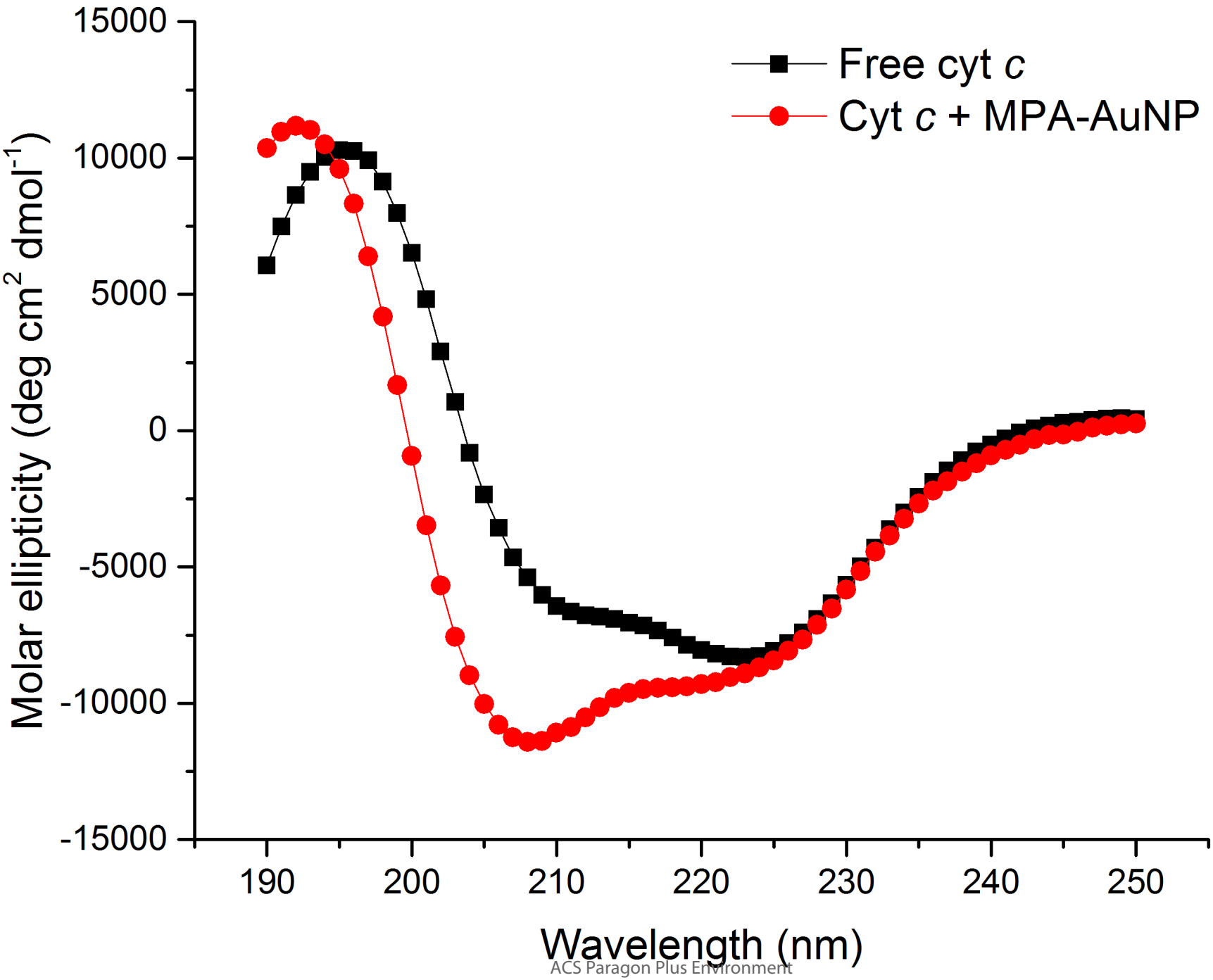
Free cyt c
Cyt c + MPA-AuNP
Molar ellipticity (deg cm2 dmol-1)
15000
10000
5000
0
-5000
-10000
-15000
190
200
210
220
230
240
250
Wavelength (nm)

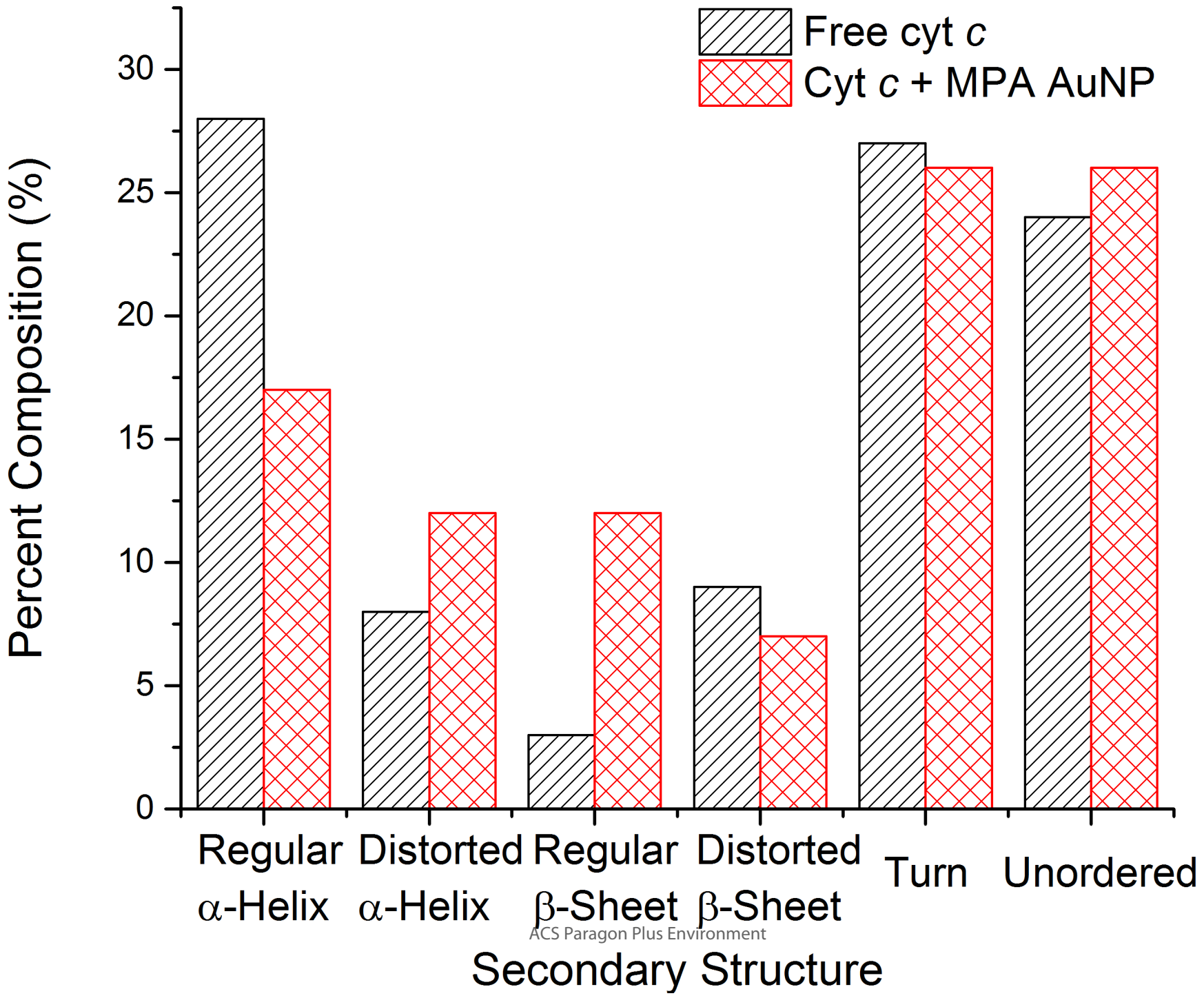

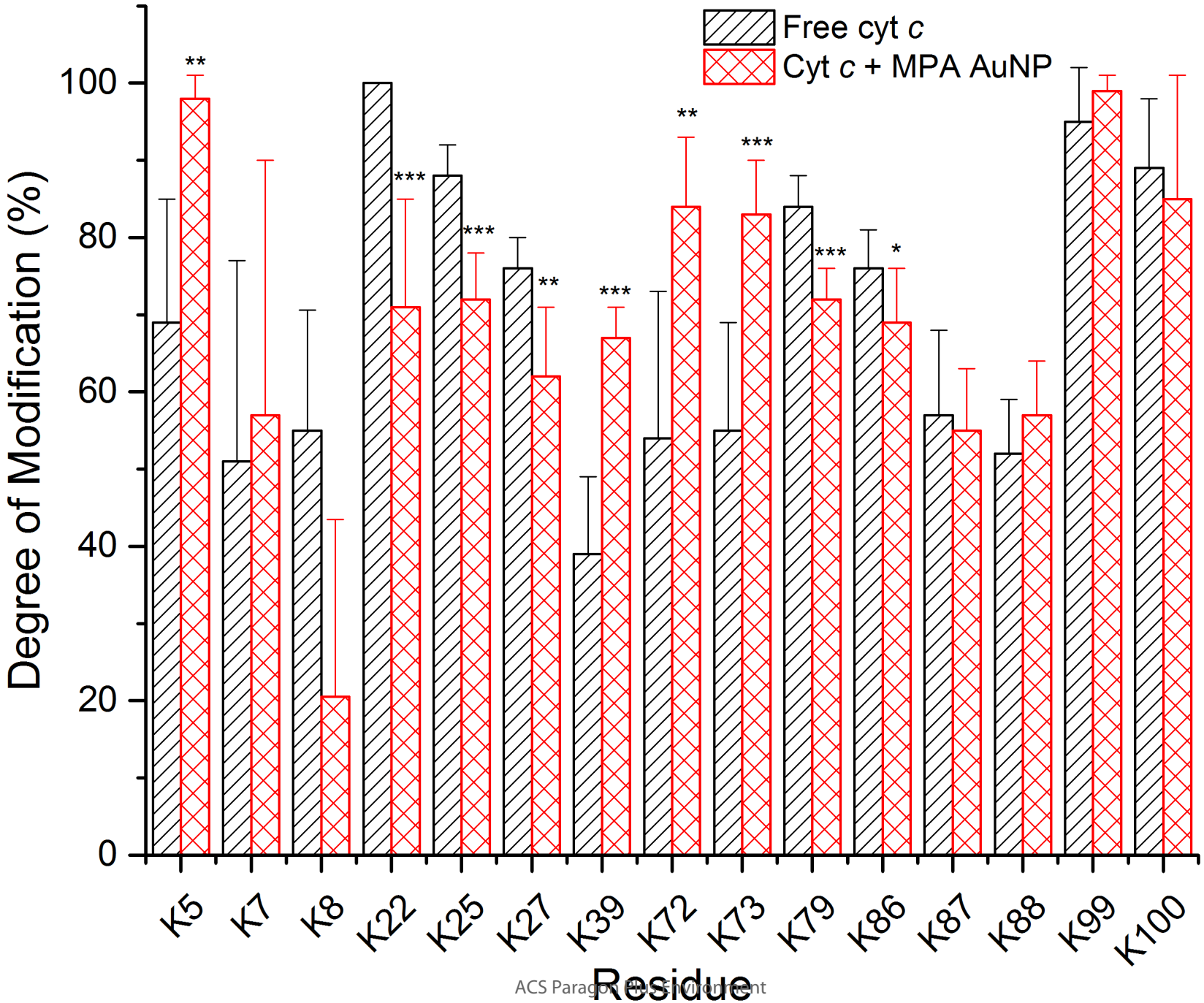

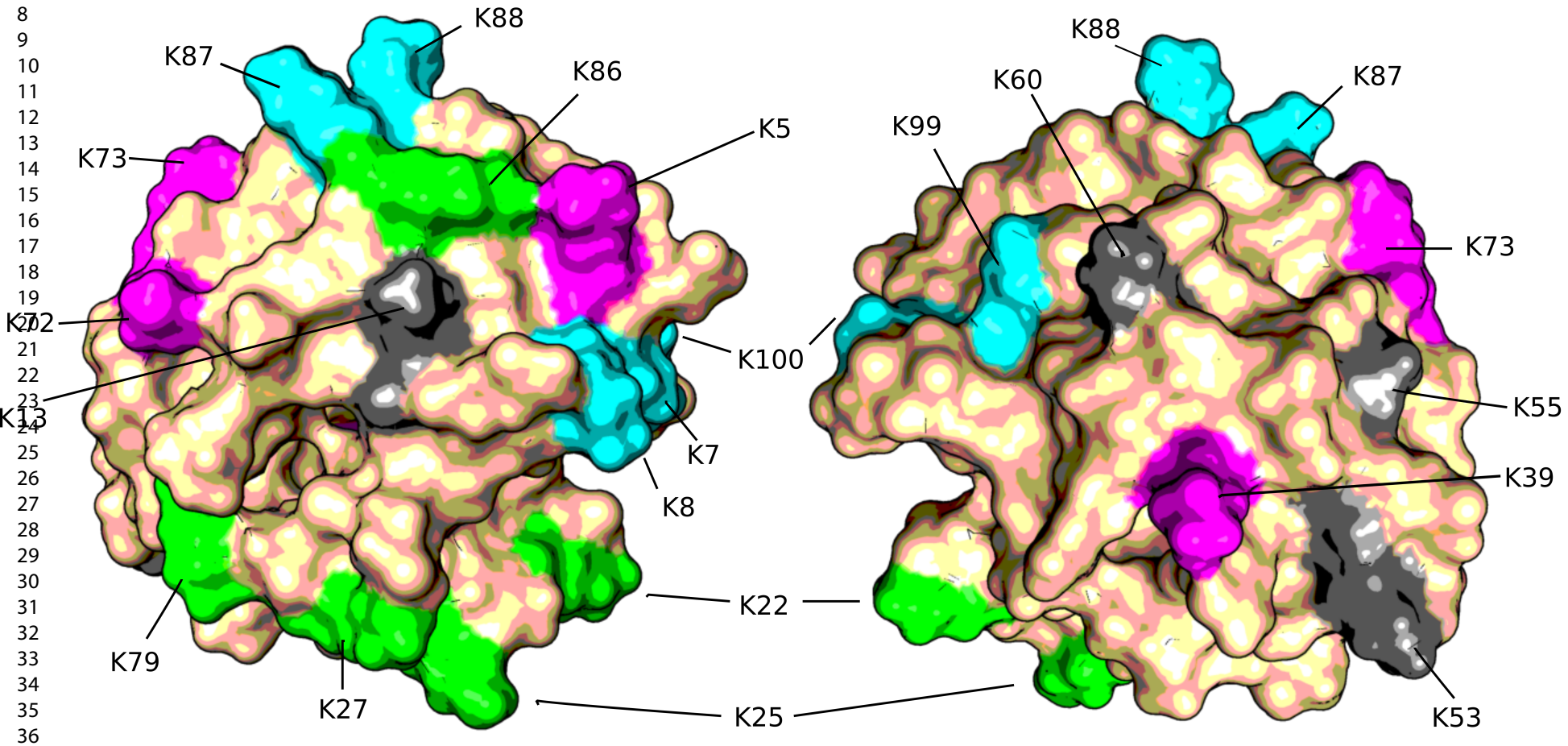
K88
K87
K86
K5
K73
K72
K13
K100
K7
K8
K79
K27
K22
K25
K88
K60
K87
K99
K73
K55
K39
K53

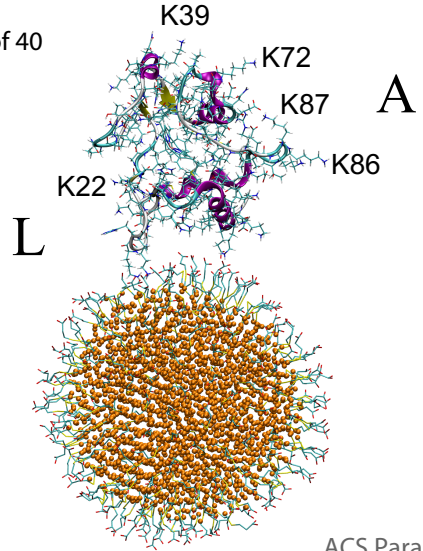
(a)
K39
K72
K87
A
K86
K22
L

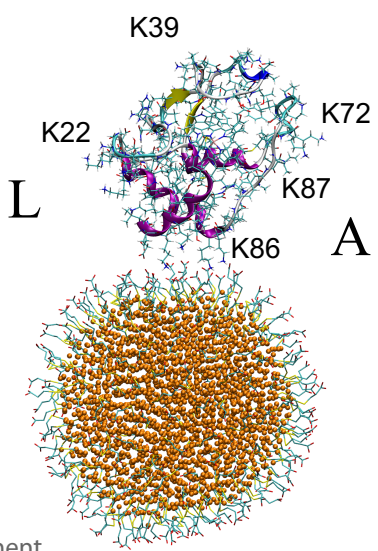
(b)
K39
K22
K72
K87
L
K86
A

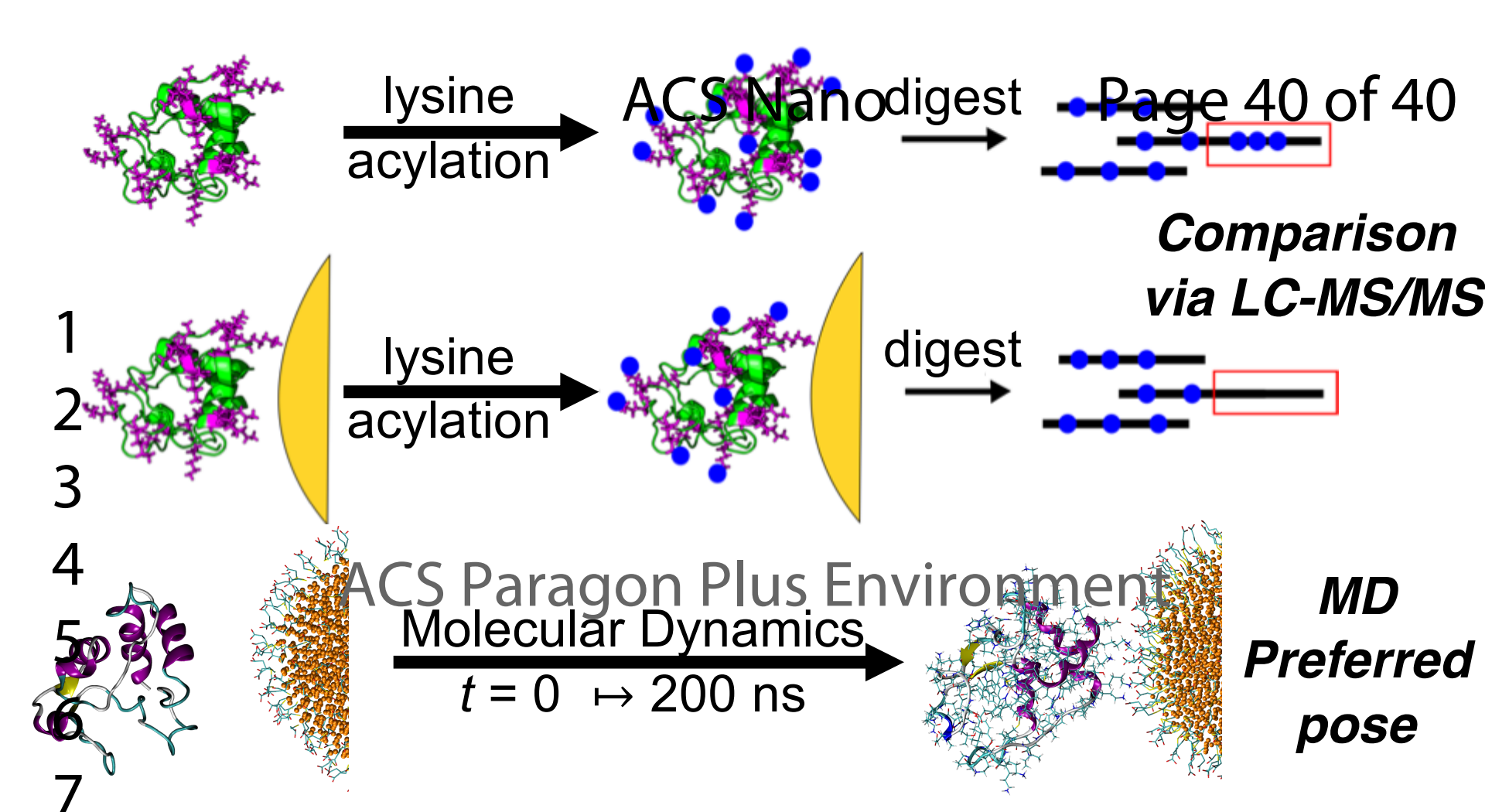
lysine
acylation
digest
Comparison
via LC-MS/MS
lysine
acylation
digest
ACS Paragon Plus Environment
Molecular Dynamics
t = 0 ↦ 200 ns
MD
Preferred
pose